Anomalous alloying behavior induced by ion irradiation in a system with a large positive heat of mixing

Z. J. Zhang,* O. Jin, and B. X. Liu*
Department of Materials Science and Engineering, Tsinghua University, Beijing 100084, China
(Received 20 June 1994; revised manuscript received 3 October 1994)

Amorphization was achieved by room temperature 200-keV xenon ion mixing in two isolated composition ranges, i.e., Y_{22}–Y_{27} and Y_{72}–Y_{83}, in the Y-Mo system, which has a positive heat of mixing exceeding +26 kJ/mol. In addition, three metastable crystalline (MX) phases, i.e., a Y-rich fcc (fcc-I), a Mo-rich hcp (hcp-I), and another fcc (fcc-II) phase, were observed at different irradiation stages. Kinetically, the fcc-I MX phase was formed through a single-step transition of hcp→fcc, while the hcp-I and fcc-II phases were formed sequentially via a two-step transition of bcc→hcp→fcc. To give further insight into the singularity of the amorphization behavior of the system and the MX phase formation, a Gibbs-free-energy diagram of the system was constructed by calculating the free energies of the amorphous phase, the solid solutions, three MX phases, and of the as-deposited Y-Mo multilayers, for which the interfacial free energies were added. The established diagram can explain well the irradiation-induced amorphization behavior and the MX phase formation in the Y-Mo system.

I. INTRODUCTION

Since the early 1980's, ion mixing (IM) has been employed as a powerful means for studying some important topics of physical metallurgy, e.g., the theory of alloy phase formation and transformation.[1] In the last decade, most research interests of IM have been focused on synthesizing amorphous alloys and studying the amorphization mechanism of the binary metal systems, especially of those with negative heats of mixing.[2–4] Using alternately deposited metals in an A and B multilayered arrangement, IM is capable of producing A_XB_{1-X} alloys without limitation of the desired alloy composition, as the relative thicknesses of A and B metals can be adjusted to obtain an arbitrary x from 0 to 1.[5] Up to date, some 70 systems have been investigated by IM of multilayers, and extensive data of the glass-forming ability (GFA) of binary metal systems have been obtained.[6] It was found that the GFA was greatly widened by IM and was continuous in composition for those systems with negative heats of mixing.[7] The amorphization behavior and GFA of systems with positive heats of mixing, however, have not yet been investigated thoroughly, and are still of interest. Recently, the formation of metastable crystalline (MX) phases has aroused enormous attention,[8] and considerable work has been carried out on the thermodynamic and kinetic aspects for a better understanding of the MX phase formation in binary metal systems mostly with negative heats of mixing.[9–11] Besides the quasicrystalline phases,[12–15] three types of MX phases have so far been observed in binary metal systems, i.e., (i) supersaturated solid solutions (SSSS);[16,17] (ii) a hexagonal phase in hcp-bcc or fcc-bcc pairs at the hcp-rich or fcc-rich side;[18–20] and (iii) a fcc phase formed in some bcc-based systems.[21] However, less attention concerning MX phase formation has been paid to systems with positive heats of mixing, leaving an open question to be further studied. The Y-Mo system, which has a positive heat of mixing exceeding +26 kJ/mol, was thus selected for this study to investigate the GFA and possible MX phase formation by IM.

Concerning the amorphization mechanism in binary metal systems, several empirical models have been proposed to predict the GFA from the crystalline structures and other static properties of the constituents and from the features of the equilibrium phase diagram,[22–24] though this problem has not been clarified on an atomic scale due to the complexity of the far-from-equilibrium nature of the IM process. Recently, a quantitative approach towards this issue has been proposed by Alonso, Gallego, and Lopez[25] on the basis of Miedema's model to calculate the free energies of the amorphous phase and the terminal solid solutions. By comparing their free-energy values, a measure of the GFA can be given under the condition of $\Delta G_a \leq \Delta G_s$, where ΔG_a and ΔG_s are the Gibbs free energies of the amorphous phase and the solid solutions, respectively.[26] This approach was quite good for the GFA in some systems. However, it cannot interpret the formation of the observed MX phases in some alloy systems,[27,28] and cannot interpret the amorphization in systems of positive heats of mixing either. Meanwhile, it has been argued that the calculation precision of the free energy is doubtful since Miedema's model and Alonso *et al.*'s method are still on a semiempirical basis. To give a precise estimation of the errors in such a calculation, however, seems quite difficult. An alternative way to step forward was recently proposed by the authors: to conduct the steady-state thermal annealing of the as-deposited multilayers to confirm the relative energetic levels of the competing phases at certain composition points.[29] Since the as-deposited multilayers are in a highly energetic state due to the additional interfacial and surface free energies, they would relax down upon annealing to the available intermediate states of lower free

energies in the system.[30] The annealing results can thus be employed to confirm the relevance of the calculated diagram in its outline.

We report, in the present paper, the detailed experimental results of amorphization and MX phase formation induced by IM in the Y-Mo system. A thermodynamic interpretation of the singularity of the amorphization behavior and MX phase formation is given by constructing the free-energy diagram of the system on the basis of Miedema's model, with the special consideration of adding the free-energy curves of the MX phases obtained in this study and that of the as-deposited Y-Mo multilayers including the interfacial free energy. The growth kinetics of the MX phases are also discussed based on the far-from-equilibrium solid-state transition upon ion irradiation.

II. EXPERIMENTAL PROCEDURE

Multilayered Y-Mo films were prepared in an evaporation system with a vacuum level on the order of 10^{-7} Torr, by depositing pure yttrium (99.9% Y) and pure molybdenum (99.9% Mo) alternately onto newly cleaved NaCl single crystals as substrates. To reduce the possible oxidation of the constituent metals, Ti was evaporated first and deposited onto a spare SiO_2 substrate to adsorb some oxygen in the vacuum system before depositing the multilayered films. During deposition, the substrates were cooled by running water and the temperature increase of the substrates was estimated to be less than 200 °C. The total thickness of the Y-Mo films was designed to match the projected range plus the projected range straggling of the irradiation ions, i.e., about 500 Å for the 200-keV xenon ions. Seven layers were deposited for each sample. The composition of the films was controlled by adjusting the relative thickness of the two constituent metals and was later confirmed by energy-dispersive-spectrum (EDS) analysis with an error of less than 5%. The as-deposited Y-Mo multilayered films were immediately moved into and kept in a dry vacuum chamber to avoid contamination. The films were then irradiated by 200-keV xenon ions in an implanter with a vacuum level on the order of 10^{-6} Torr. The beam current density was controlled to be less than 0.5 $\mu A/cm^2$ to minimize beam heating effects, and the temperature increase of the substrates was estimated to be less than 100 °C. After irradiation, all the mixed films were removed from the substrates by deionized water and put on Cu or Mo grids for transmission electron microscopy (TEM) observation and selected-area diffraction (SAD) analysis to identify the structure. EDS was also employed to determine the real composition of the ion-mixed phases. Some as-deposited multilayered films were subjected to steady-state thermal annealing in a hot stage attached to the TEM, which had a vacuum level on the order of 10^{-7} Torr, to give an independent result of phase evolution for testing the validity of the calculated free-energy diagram.

III. RESULTS AND DISCUSSION

A. Amorphization induced by IM

Table I lists the phase changes in the Y-Mo system induced by room-temperature 200-keV xenon ion mixing as a function of irradiation doses. From the table, one sees that at the Y-rich side, Y_{83}-Mo_{17} films were amorphized at a dose of 1×10^{15} Xe^+/cm^2 and that the $Y_{72}Mo_{28}$ films were also amorphized at a dose of 3×10^{15} Xe^+/cm^2. Figures 1(a)–(d) show the bright-field images and the corresponding SAD patterns of the as-deposited and amorphized $Y_{72}Mo_{28}$ multilayered films. Meanwhile, at the Mo-rich side, $Y_{22}Mo_{78}$ and $Y_{27}Mo_{72}$ films were both amorphized at a dose of 1×10^{15} Xe^+/cm^2. Figures 2(a) and 2(b) show the SAD patterns of the as-deposited and amorphized $Y_{22}Mo_{78}$ multilayered films, respectively. In the other samples, i.e., $Y_{15}Mo_{85}$, $Y_{42}Mo_{58}$, and $Y_{65}Mo_{35}$ films, amorphization was not achieved at any irradiation doses, i.e., from 3×10^{14} to 7×10^{15} Xe^+/cm^2. These results suggest that amorphization can be achieved, yet in two isolated composition ranges in the Y-Mo system by IM.

B. Formation of the MX phases

The Y-rich $Y_{83}Mo_{17}$ films were amorphized at a dose of 1×10^{15} Xe^+/cm^2, and transformed into a fcc-I phase at a dose of 7×10^{15} Xe^+/cm^2. For the $Y_{72}Mo_{28}$ films, amorphization was achieved at a dose of 3×10^{15}

TABLE I. Phase changes in the Y-Mo multilayers induced by room-temperature 200-keV xenon ion mixing. (The dosages are in 10^{14} Xe^+/cm^2; "*A*" stands for amorphous phase; "bcc" is a Mo-rich solid solution; "hcp-I," "fcc-I," and "fcc-II" are three MX phases). The ion-induced phase formation in the $Y_{27}Mo_{73}$ multilayer was quite similar to that in the $Y_{22}Mo_{78}$ films and was thus not listed in the table.

Dosage	$Y_{15}Mo_{85}$	$Y_{22}Mo_{78}$	$Y_{42}Mo_{58}$	$Y_{65}Mo_{35}$	$Y_{72}Mo_{28}$	$Y_{83}Mo_{17}$
3	Y+Mo	Y+Mo	Y+Mo	Y+Mo	Y+Mo	Y+Mo
5	Y+Mo	Y+Mo	Y+Mo	Y+Mo	Y+Mo	Y+Mo
7	Y+Mo	Y+Mo	Y+Mo	Y+Mo	Y+Mo	Y+Mo
10	bcc	*A*	Y+Mo	Y+Mo	Y+Mo	*A*
30	hcp-I	hcp-I	Y+Mo	Y+Mo	*A*	*A*
50	hcp-I+fcc-II	hcp-I+fcc-II	Y+Mo	Y+Mo	*A*	*A*
70	fcc-II	fcc-II	Y+Mo	Y+Mo	fcc-I	fcc-I

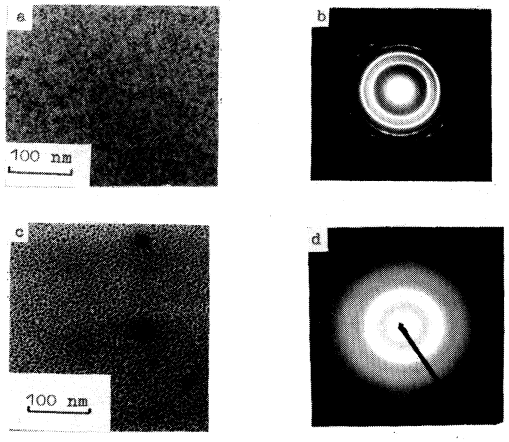

FIG. 1. (a) and (b) show a bright-field image and a corresponding SAD pattern of the as-deposited $Y_{72}Mo_{28}$ multilayers; (c) and (d) show a typical bright image and the corresponding SAD pattern of the amorphized multilayers at an irradiation dose of 3×10^{15} Xe^+/cm^2 by room-temperature 200-keV xenon ion mixing.

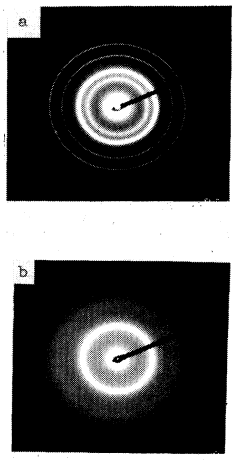

FIG. 2. (a) and (b) are the SAD patterns of the as-deposited $Y_{22}Mo_{78}$ multilayers and the corresponding amorphous phase formed by 200-keV room-temperature xenon ion mixing to a dose of 1×10^{15} Xe^+/cm^2.

Xe^+/cm^2 [see Fig. 1(d)], and turned into a fcc-I phase at a higher dose of 7×10^{15} Xe^+/cm^2. Figures 3(a) and 3(b) show a typical bright-field image and the corresponding SAD pattern of the fcc-I phase, respectively. The lattice parameter of the fcc-I phase was determined to be $a=5.10$ Å. Table II lists the indexing results for the fcc-I phase. The formation of the fcc-I phase can therefore be viewed via an ion-induced transition of

$$Y_{72}Mo_{28}\xrightarrow[RT]{1\times10^{15}\ Xe^+/cm^2}\text{amorphous}\xrightarrow[RT]{7\times10^{15}\ Xe^+/cm^2}\text{fcc-I}\ . \tag{1}$$

At the Mo-rich side, when the $Y_{15}Mo_{85}$ films were irradiated to a dose of 1×10^{15} Xe^+/cm^2, the structure of the films was bcc, indicating the formulation of a Mo-rich solid solution. The films were changed into a hcp structure (hcp-I phase) at a dose of 3×10^{15} Xe^+/cm^2. The lattice parameters of the hcp-I phase were identified to be $a=2.89$ Å and $c=4.70$ Å. Table III lists the indexing results of the hcp-I phase. When the films were irradiated to a dose of 5×10^{15} Xe^+/cm^2, a mixture of the hcp-I and a new fcc-II phase was observed. When the films were irradiated to a dose of 7×10^{15} Xe^+/cm^2, a unique fcc-II phase was formed. Figures 4(a)–4(f) are a typical bright image and a corresponding SAD pattern of the as-deposited $Y_{15}Mo_{85}$ films, and the SAD patterns of the films at different irradiation stages. The lattice parameter of the fcc-II phase was determined to be $a=4.04$ Å. Table IV is the identification of the fcc-II phase. Similar results were also obtained in the $Y_{27}Mo_{73}$ and $Y_{22}Mo_{78}$ films at respective irradiation stages. These results can therefore be summarized as follows:

$$Y_{15}Mo_{85}\xrightarrow[RT]{1\times10^{15}\ Xe^+/cm^2}\text{bcc}\xrightarrow[RT]{3\times10^{15}\ Xe^+/cm^2}\text{hcp-I}\xrightarrow[RT]{7\times10^{15}\ Xe^+/cm^2}\text{fcc-II}\ . \tag{2}$$

TABLE II. Identification of the Y-rich fcc-I MX phase formed in the $Y_{83}Mo_{17}$ multilayers by 200-keV xenon ion mixing to a dose of 7×10^{15} Xe^+/cm^2 at room temperature. $a=5.10$ Å.

$d_{\text{experimental}}$ (Å)	(hkl)	$d_{\text{calculation}}$ (Å)	$\lvert\Delta d\rvert$ (Å)	Intensity
2.93	111	2.94	0.01	strong
2.54	200	2.55	0.01	strong
1.81	220	1.80	0.01	strong
1.53	311	1.54	0.01	strong
1.45	222	1.47	0.02	medium
1.26	400	1.28	0.02	medium
1.17	331	1.17	0.00	medium
1.12	420	1.14	0.02	weak

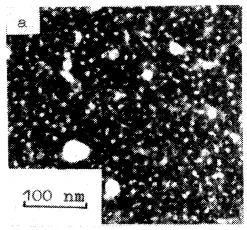

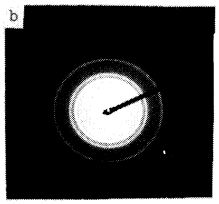

FIG. 3. (a) and (b) show a typical bright image and a corresponding SAD pattern of the Y-rich fcc-I MX phase formed in the $Y_{83}Mo_{17}$ multilayers by 200-keV xenon ion mixing to a dose of 7×10^{15} Xe^+/cm^2 at room temperature.

Note that "bcc" is a Mo-rich solid solution.

It should be pointed out that the Y-rich fcc-I and Mo-rich hcp-I and fcc-II phases were metastable crystalline phases in the Y-Mo system since their diffraction lines could not be indexed to either those of the elemental metals or those of the possible Y, Mo, and (Y+Mo) oxides.

C. Thermodynamic interpretation

1. Survey of theory

Generally, the Gibbs free energy of a phase is calculated by $\Delta G=\Delta H\text{-}T\Delta S$, where ΔH and ΔS are the enthalpy and entropy terms, respectively. As a first approximation, the entropy term for a solid solution for an amorphous phase is simply taken as that of an ideal solid solution, i.e.,

$$\Delta S=-R[X_A\ln(X_A)+X_B\ln(X_B)]\ ,$$

in which R is the gas constant and X_A and X_A are atomic concentrations of A and B metals, respectively. According to Miedema, Chatel, and De Boer, the enthalpy change ΔH can be considered as a sum of three terms,

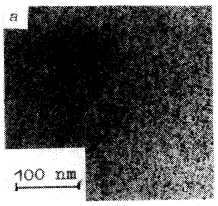

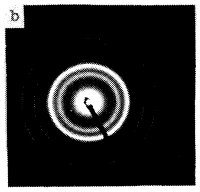

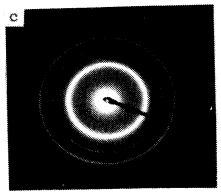

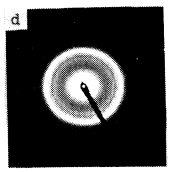

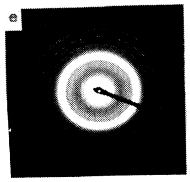

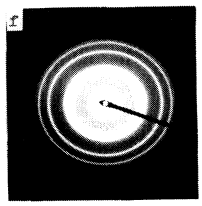

FIG. 4. (a),(b) Morphology and corresponding SAD pattern of the as-deposited $Y_{15}Mo_{85}$ multilayered films. (c)–(f) are the SAD patterns of the films at different irradiation stages upon 200-keV xenon ion mixing at room temperature: (c) a bcc solid solution formed at 1×10^{15} Xe^+/cm^2; (d) a hcp-I MX phase formed at 3×10^{15} Xe^+/cm^2; (e) a mixture of (hcp-I + fcc-II) formed at a dose of 5×10^{15} Xe^+/cm^2; and (f) a unique fcc-II MX phase formed at 7×10^{15} Xe^+/cm^2.

i.e., $\Delta H=\Delta H^c+\Delta H^e+\Delta H^s$, corresponding to the chemical, elastic, and structural contributions. The chemical term ΔH^c is closely related to the electron redistribution generated at the boundary for the Wigner-Seitz unit cell when alloying, the elastic term ΔH^e is caused by the atomic size mismatch of the two constituent metals, while the structural term ΔH^s is deduced from the valence and crystal-structure changes.[31,32] These terms for the solid solutions, the amorphous phase, and the intermetallic compound can easily be calculated following

TABLE III. Indexing results of the Mo-rich hcp-I MX phase formed in the $Y_{15}Mo_{85}$ multilayers under 200-keV room-temperature xenon ion mixing to an irradiation dose of 3×10^{15} Xe^+/cm^2. $a=2.89$ Å, $c=4.70$ Å, and $c/a=1.63$.

$d_{\text{experimental}}$ (Å)	(hkl)	$d_{\text{calculation}}$ (Å)	$\lvert\Delta d\rvert$ (Å)	Intensity
2.52	100	2.50	0.02	medium
2.35	002	2.35	0.00	strong
2.22	101	2.21	0.01	strong
1.70	102	1.71	0.01	strong
1.44	110	1.45	0.01	strong
1.32	103	1.33	0.01	medium
1.23	112	1.23	0.00	medium
1.05	104	1.06	0.01	weak

the well-documented literature.[33] These terms for the MX phase, however, should be discussed in detail.

First, a MX phase is of an ordered structure, and the entropy term can be ignored since it only has a minor effect on the free-energy change just like that of an ordered equilibrium compound. The Gibbs-free-energy change of a MX phase is therefore

$$\Delta G_{\mathrm{MX}}=\Delta H^{c}_{\mathrm{MX}}+\Delta H^{s}_{\mathrm{MX}}+\Delta H^{s}_{\mathrm{MX}} , \tag{3}$$

where the three terms at the right side are chemical, elastic, and structural contributions of the MX phase, respectively. The chemical term $\Delta H^{c}_{\mathrm{MX}}$ is accordingly calculated by

$$\Delta H^{c}_{\mathrm{MX}}=\Delta H_{\mathrm{amp}} X_A V_A^{2/3} f_{AB} , \tag{4}$$

where ΔH_{amp} is an amplitude and is a constant for a specific system, e.g., $+16.5$ kJ/mol cm^2 for the Y-Mo system. X_A and V_A are the atomic concentration and volume of atom A. f_{AB} is a function, namely, the extent of atom A surrounded by atom B. In the calculation of f_{AB}, a constant γ is used to describe the chemical short-range-order (CSRO) difference of the solid solutions, the amorphous phase, and the ordered compound. The values of γ are empirically taken as 0, 5, and 8 for the solid solution, the amorphous phase, and the compound, respectively.[34] As a MX phase is commonly considered as compoundlike, it is reasonable to assume that the CSRO in the MX phase is similar to that in an ordered compound. The value of γ is therefore taken as 8 for the MX phase.

Secondly, the elastic term of a MX phase is related to the lattice distortion caused by the size mismatch between the two constituent metals.[35] It is well known, however, that in an equilibrium compound the elastic energy can be neglected, since the lattice distortion caused by the atomic size mismatch of the two constituent metals can be relaxed down to a minimum by the ordered arrangement of the atoms. If a MX phase is formed near the eutectic point, where no corresponding equilibrium compound exists, the elastic term of the MX phase is negligible as the ordered arrangement of atoms in it can relax the lattice distortion to a minimum. Yet for a MX phase formed at a composition near an equilibrium compound, the elastic term of the MX phase cannot be neglected, as the structure and the atomic arrangement of the MX phase are different from that of the equilibrium compound and thus cannot relax the lattice distortion to a minimum. The elastic term for this MX phase is therefore

$$\Delta H^{e}_{\mathrm{MX}}=X_A X_B[X_A \Delta H^{e}_{\mathrm{MX}(B \text{ in } A)}+X_B \Delta H^{e}_{\mathrm{MX}(A \text{ in } B)}] , \tag{5}$$

where $\Delta H^{e}_{\mathrm{MX}(i \text{ in } j)}$, is the elastic contribution to the heat of solution of i in j in the MX phase, and can be calculated by the method proposed by de Boer, Miedema, and Boom.[36] It is worth mentioning that this formula can also be used to calculate the elastic term of the solid solution, but the values of the heat of solution $\Delta H_{(i \text{ in } j)}$ are different from those of $\Delta H^{e}_{\mathrm{MX}\ (i \text{ in } j)}$. For the Y-Mo system, $\Delta H^{e}_{(\mathrm{Y \text{ in } Mo})}$ and $\Delta H^{e}_{(\mathrm{Mo \text{ in } Y})}$ are $+56$ and $+131$ kJ/mol, respectively.[37] The values of $\Delta H^{e}_{\mathrm{MX}(i \text{ in } j)}$ for the fcc-I, hcp-I, and fcc-II phases were also calculated and listed in Table V for comparison.

Thirdly, the structure of a MX phase is different from the constituent metals, and thus the difference in structure has a contribution to the free-energy change. The structural contribution is then[7]

$$\Delta H^{s}_{\mathrm{MX}}=E(Z)-X_A E(Z_A)-X_B E(Z_B) , \tag{6}$$

where $E(Z)$, $E(Z_A)$, and $E(Z_B)$ are the lattice stability of the MX phase and pure A and B metals, and Z, Z_A, and Z_B are the mean number of valence electrons of the MX phase and the number of valence electrons of pure metals A and B, respectively.[38] The dependence of the lattice stability on Z for paramagnetic and ferromagnetic transition metals has been calculated by Niessen *et al.*[39]

According to above discussion, the Gibbs-free-energy change of a MX phase can be classified into two types, (i) for a MX phase formed at a composition in the vicinity of an equilibrium compound,

$$\Delta G_{\mathrm{MX}}=\Delta H^{c}_{\mathrm{MX}}+\Delta H^{e}_{\mathrm{MX}}+\Delta H^{s}_{\mathrm{MX}} , \tag{7}$$

and (ii) for a MX phase formed at a composition near the eutectic point where no corresponding compound exists,

$$\Delta G_{\mathrm{MX}}=\Delta H^{c}_{\mathrm{MX}}+\Delta H^{s}_{\mathrm{MX}} . \tag{8}$$

Accordingly, the Gibbs-free-energy changes of the Y-rich and Mo-rich solid solutions, the Y-Mo amorphous phases, and the fcc-I, hcp-I, and fcc-II MX phases were calculated. The values of the parameters used in the cal-

TABLE IV. Identification of the Mo-rich fcc-II MX phase formed in the $Y_{15}Mo_{85}$ multilayers upon room-temperature 200-keV xenon ion mixing to a dose of 7×10^{15} Xe$^+$/cm^2. $a=4.04$ Å.

$d_{\mathrm{experimental}}$ (Å)	(hkl)	$d_{\mathrm{calculation}}$ (Å)	$\lvert\Delta d\rvert$ (Å)	Intensity
2.30	111	2.33	0.03	strong
2.01	200	2.02	0.01	strong
1.42	220	1.43	0.01	strong
1.24	311	1.22	0.02	strong
1.16	222	1.17	0.01	medium
1.02	400	1.01	0.01	medium
0.92	331	0.93	0.01	medium
0.89	420	0.90	0.01	weak

TABLE V. Values of the parameters used in calculating the free-energy diagram of the Y-Mo system and the free energy of the as-deposited Y-Mo multilayered films. (Note that " · · · " means the data were not used, "films" stands for the as-deposited Y-Mo films, the unit of ΔH_{amp} is kJ/mol m^2, and the unit of $\Delta H_{(i \text{ in } j)}$ and $\Delta H^0_{(i \text{ in } j)}$ is kJ/mol.)

Parameter	Y	Mo	SS	A	fcc-I	hcp-I	fcc-II	Films
V (cm^3)	19.89	9.39	· · ·	· · ·	· · ·	· · ·	· · ·	· · ·
γ	· · ·	· · ·	0	5	8	8	8	· · ·
ΔH_{amp}	· · ·	· · ·	16.5	16.5	16.5	16.5	16.5	· · ·
$\Delta H^0_{(Y \text{ in Mo})}$	· · ·	· · ·	56	· · ·	67	44	44	56
$\Delta H_{(Mo \text{ in Y})}$	· · ·	· · ·	131	· · ·	172	127	127	131
γ^0 (mJ/m^2)	3000	1125	· · ·	· · ·	· · ·	· · ·	· · ·	· · ·
$\Delta H_{(Y \text{ in Mo})}$	· · ·	· · ·	114	114	114	114	114	114
$\Delta H^0_{(Mo \text{ in Y})}$	· · ·	· · ·	81	81	81	81	81	81
s_f (10^{5}m^2)	3.3	2.0	· · ·	· · ·	· · ·	· · ·	· · ·	· · ·

culation were listed in Table V. Figure 5 shows a calculated Gibbs-free-energy diagram of the Y-Mo system.

2. *Steady-state thermal annealing results*

Steady-state thermal annealing of some as-deposited multilayered films was conducted with increasing temperature. At the Y-rich side, the $Y_{72}Mo_{28}$ films were first amorphized after annealing at 250 °C for 1$\frac{1}{2}$h, and then turned into the fcc-I phase when the temperature reached 350 °C and held for $\frac{1}{2}$ h. Further annealing at a higher temperature of 600 °C for 1 h caused the transformation from the fcc-I phase into a mixture of Y+Mo. Figures 6(a)–6(d) show the SAD patterns of the $Y_{72}Mo_{28}$ films at different annealing stages. In the Mo-rich $Y_{22}Mo_{78}$ multilayered films, a hcp-I phase was first formed when the films were annealed at a temperature of 500 °C for about an hour, and then the hcp-I phase changed into the fcc-II phase on annealing at a higher temperature of 600 °C for one more hour. The fcc-II phase is very stable upon further annealing up to 800 °C. Figures 7(a)–7(c) show the SAD patterns of the as-deposited $Y_{22}Mo_{78}$ films and the formed hcp-I and fcc-II phases, respectively. The annealing results of the Y-rich and Mo-rich films can be summarized as

$$Y_{72}Mo_{28}\frac{250\,^\circ\text{C}}{90\text{ min}}>\text{amorphous}\frac{350\,^\circ\text{C}}{30\text{ min}}$$
$$>\text{fcc-I}\frac{600\,^\circ\text{C}}{60\text{ min}}>\text{Y+Mo}\ , \tag{9}$$

$$Y_{22}Mo_{78}\frac{500\,^\circ\text{C}}{60\text{ min}}>\text{hcp-I}\frac{600\,^\circ\text{C}}{60\text{ min}}>\text{fcc-II}\ . \tag{10}$$

From the phase appearance sequence upon steady-state thermal annealing just mentioned, it is obvious that the Y-rich fcc-I and Mo-rich hcp-I and fcc-II phases were indeed metastable phases in the Y-Mo system, and that the Y-rich fcc-I phase has lower free energy than the

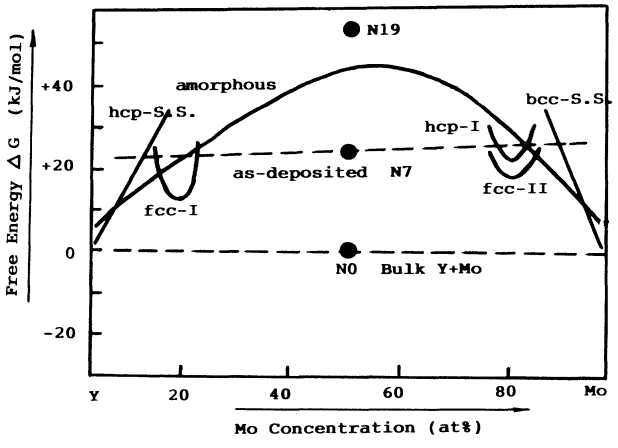

FIG. 5. A typical calculated Gibbs-free-energy diagram of the Y-Mo system. The dashed line shows the initial energetic levels of the as-deposited multilayers. N19 and N7 indicate samples with 19 and seven layers, respectively.

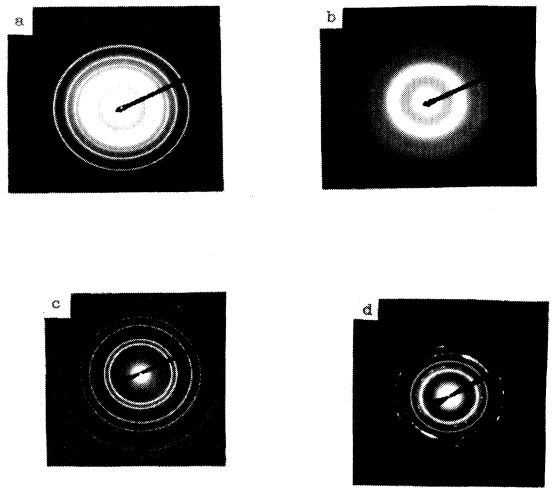

FIG. 6. SAD patterns of the $Y_{72}Mo_{28}$ multilayered films upon steady-state thermal annealing: (a) as deposited; (b) amorphized at 250 °C for 90 min; (c) the fcc-I MX phase formed after annealing at 350 °C for 30 min; and (d) the (Y+Mo) mixture reemerged when the temperature reached 600 °C and stayed for 60 min.

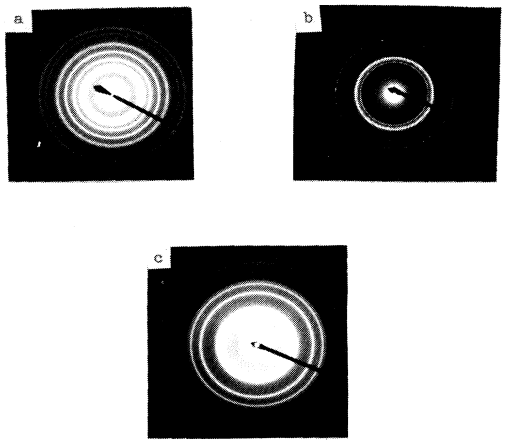

FIG. 7. SAD patterns of the $Y_{22}Mo_{78}$ multilayered films at different annealing stages: (a) as deposited; (b) the hcp-I MX phase formed after annealing at 500 °C for 60 min; and (c) the fcc-II MX phase formed after further annealing at 600 °C for 60 min.

corresponding amorphous phase, the Mo-rich fcc-II has lower free energy than the hcp-I one. These results are in agreement with the calculated free-energy diagram, and thus confirm the relevance of the calculated free-energy diagram in its outline.

3. *Interpretation to the GFA and MX phase formation*

a. The influence of the interfaces on the GFA. First, we focus on the GFA in the Y-Mo system. From Fig. 5, one may notice that the free-energy curves of the Y-rich, Mo-rich, and amorphous phases are convex in their shapes, and the amorphous phase has lower free energies than the two terminal solid solutions within a wide composition range, i.e., Y_{12}–Y_{87}. According to Alonso, Gallego, and Somozar,[20] the possible GFA of the Y-Mo system is Y_{12}–Y_{87}. Experimentally, however, the Y-Mo amorphous phase has so far been obtained in two isolated composition ranges, i.e., Y_{22}–Y_{27} and Y_{72}–Y_{83}. It should be pointed out that at the compositions near the equiatomic stoichiometry, e.g., $Y_{45}Mo_{55}$ films, amorphization was not achieved, unlike in most of the previous results obtained in systems of negative heats of mixing.[40,41] From Fig. 5, it can be seen that both the solid solutions and the amorphous phases are thermodynamically unstable, as their free energies are much higher than that of a mixture of the two pure constituents.

It is well known that multilayered films consisting definitely of a certain number of interfaces can exist in a state of higher free energy than that of the corresponding bulk counterpart, as the interfaces can give a rise to an additional interfacial free energy.[42] The additional interfacial free energy, in some cases, may elevate the multilayers to a state of higher free energy than that of the amorphous state, and thus serves as a major driving force for the formation of some new phases.[43] According to Gerkema and Miedema[44] the interfacial free energy is

$$\Delta G_{[A]-[B],f}=S_f\times\gamma^{AB}\ , \tag{11}$$

where $\Delta G_{[A]-[B],f}$ is the interfacial free energy of a B atom on the A-atom layer, S_f is the surface area occupied by one mole of interfacial atoms, and γ^{AB} is a constant for a specific system and can be calculated by[44]

$$\gamma^{AB}=0.15(\gamma_A^0+\gamma_B^0)+\gamma_{AB}^{\text{chem}}\ , \tag{12}$$

where γ_A^0 and γ_B^0 are the surface energies of solid A and solid B, e.g., $\gamma_Y^0=+1125$ mJ/m^2, and $\gamma_{Mo}^0=+3000$ mJ/m^2. $\gamma_{AB}^{\text{chem}}$ is the chemical contribution concerning the reaction between A and B atoms. It is worth mentioning that the first part at the right side of Eq. (12) is the elastic term caused by mismatch of atomic sizes. According to Gerkema and Miedema $\gamma_{AB}^{\text{chem}}$ is a constant for a specific system and is given by $\gamma_{AB}^{\text{chem}}=\Delta H^0_{(A\text{ in }B)}/(c_0V_A^{2/3})$, where c_0 is a constant being 4.5×10^8, and $\Delta H^0_{(A\text{ in }B)}$ is a constant for a specific system, e.g., $\Delta H^0_{(Y\text{ in Mo})}=+114$ kJ/mol and $\Delta H^0_{(Mo\text{ in Y})}=+81$ kJ/mol for the Y-Mo system.

Figure 8 shows schematically the configuration of A-B multilayers. Suppose N_A and N_B are numbers of layers of metal A and B, $d_{A,i}$ and $d_{B,j}$ are the thicknesses of the ith layer of A and B, and $\Delta d_{A,i}$ and $\Delta d_{B,i}$ are the thicknesses of the ith interface of (A on B) and (B on A), respectively. Then the interfacial atoms are a fraction of total atoms,

$$\alpha=X_A\frac{\sum_i^{nA}\Delta d_{A,i}}{\sum_i d_{A,i}}+X_B\frac{\sum_i^{nB}\Delta d_{B,i}}{\sum_i d_{B,i}}\ . \tag{13}$$

In the formula, α is the fraction and n_A and n_B are the numbers of (A on B) interfaces and (B on A) interfaces, respectively. Obviously, n_A and n_B should match the relationship of $(n_A+n_B)+1=N_A+N_B$. For simplicity, the thicknesses of the interfaces, i.e., Δd_Y and Δd_{Mo}, were taken as a constant, being 5 Å in the calculation.[45] Formula (13) is then rewritten as $\alpha=\alpha_A=\alpha_B$, where

$$\alpha_A=X_A\frac{\sum_i^{nA}\Delta d_{A,i}}{\sum_i d_{A,i}}\quad\text{and}\quad\alpha_B=X_B\frac{\sum_i^{nB}\Delta d_{Bi}}{\sum_i d_{B,i}}\ . \tag{14}$$

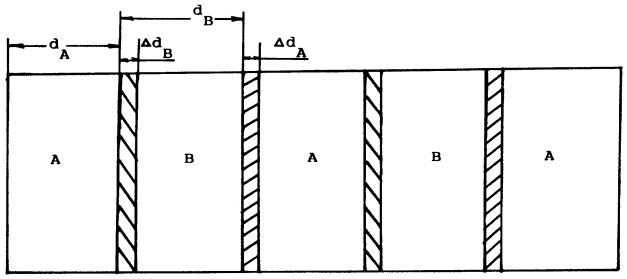

FIG. 8. Configuration of A and B component metals in an alternately deposited multilayered film. The thicknesses of the A and B layers and the (A on B) and (B on A) interfaces are shown schematically.

The interfacial free energies for the multilayers can then be calculated by

$$\Delta G_f = \alpha_A S_{fA} \gamma^{BA} + \alpha_B S_{fB} \gamma^{AB} , \quad (15)$$

where $S_{fY} = 3.3 \times 10^5$ m^2 and $S_{fMo} = 2.0 \times 10^5$ m^2, respectively.

The interfacial free energies for the as-deposited Y-Mo multilayered films were therefore calculated and the free-energy curve of the Y-Mo multilayers was added in Fig. 5 as a dashed line, representing the initial energy level of the as-deposited Y-Mo multilayers. Comparing with the free-energy curve of the amorphous phase, it is obvious that within the composition range of Y_{21}–Y_{78} the amorphous alloy has higher free energy than the as-deposited films, suggesting that the amorphous phase is thermodynamically unfavored in the present case as there is no driving force responsible for amorphous phase formation in this composition range. Under the condition of $\Delta G_s \geq \Delta G_a \leq \Delta G_m$, where ΔG_m is the free energy of the multilayered films, the composition range favoring amorphization can be deduced from Fig. 5 to be Y_{10}–Y_{21} and Y_{78}–Y_{88}, which agrees with the experimental ones, i.e., Y_{22}–Y_{27}, and Y_{72}–Y_{83}.

The next issue is the possibility of amorphization in the system at compositions around equiatomic stoichiometry by artificially adding extra interfaces into the Y-Mo multilayered films. To demonstrate the significant effect of the interfaces on amorphization behavior in a system with large positive heat of mixing like the Y-Mo system, two samples of $Y_{50}Mo_{50}$ multilayers with 19 layers (N19) and with seven layers (N7) were deposited and then annealed *in situ* in the hot stage attached to the TEM for comparison. It was found that the N19 sample was indeed amorphized after annealing at 350 °C for 2 h, and then transformed into a mixture of Y+Mo at a temperature of 650 °C. For the N7 multilayered films, the structure was a mixture of crystalline Y and Mo and remained unchanged up to a temperature as high as 800 °C. Figures 9(a)–(d) are a morphology and a corresponding SAD pattern of the as-deposited N19 multilayers and SAD patterns of the amorphous phase and Y+Mo mixture, respectively, after annealing. These results indicate that the amorphous phases, which are thermodynamically unstable in systems of positive heats of mixing, can be formed by thermal annealing of the multilayers, if the interfacial free energy is large enough, e.g., the N19 films. Accordingly, the initial energetic levels of the N19 and N7 multilayers were calculated, and were labeled by solid circles in Fig. 5. Obviously, it is the interfaces that elevated the multilayered films to a state of higher free energy than that of the bulk state, and in some cases elevated the state of the multilayered films to be higher than the amorphous one, as demonstrated by the N19 multilayered films. As a consequence, the excess free energy originating from the interfaces was responsible for the amorphous phase formation in the system by providing the thermodynamic driving force. In other words, the amorphous phase formation in the Y-Mo system with a rather positive heat of mixing was actually interface generated.

b. Thermodynamic interpretation of the MX phase formation. We now discuss the formation of the Y-rich fcc-I and Mo-rich hcp-I and fcc-II phases. It is clear from Fig. 5 that the three phases have lower free energies than that of the N7 films, and are therefore thermodynamically favored compared with the multilayered films. Besides, one can also see from the figure that the fcc-I phase has lower free energies at compositions around $Y_{80}Mo_{20}$ than both the Y-rich solid solution and the amorphous phase. For the Mo-rich hcp-I and fcc-II MX phases, the calculation illustrates that around $Y_{20}Mo_{80}$, the hcp-I and fcc-II phases are more stable than the Mo-rich solid solution and the amorphous phase, and the fcc-II phase is the most stable one among them, while hcp-I is the second most stable one. The possible emergence sequences of the related phases can thus be deduced from the calculated free-energy diagram as

$$Y_{80}Mo_{20} \rightarrow \text{amorphous} \rightarrow \text{fcc-I}$$

and

$$Y_{20}Mo_{80} \rightarrow \text{amorphous} \rightarrow \text{hcp-I} \rightarrow \text{fcc-II}$$

The deductions agree fairly well with the experimental results.

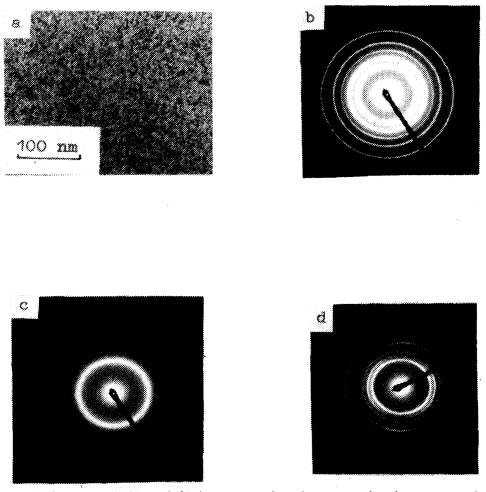

FIG. 9. (a) and (b) exhibit a typical morphology and a corresponding SAD pattern of the as-deposited N19 sample; (c) and (d) are the SAD patterns of the amorphized N19 sample at 350 °C, and the reemerged (Y+Mo) mixture at 650 °C, respectively.

4. Structural compatibility between the MX phases and the matrix

The above calculations revealed the thermodynamic driving force for the formation of the fcc-I, hcp-I, and fcc-II phases. The next question is then how the three MX phases were formed under the restricted kinetic conditions available in IM. IM is generally recognized to be a two-step nonequilibrium process, i.e., first an atomic collision cascade and then a relaxation period lasting for only 10^{-10}–10^{-9} s, within which the structure of the newly formed phases was expected to grow. As a result, the alloy phase formed upon ion irradiation can only be of a simple crystalline structure or an amorphous struc-

ture, because such a short span of time prevents the nucleation and growth of a complicated structured phase as long-range diffusion is impossible.[46] Accordingly, only those fast and partitionless transition mechanisms can be executed. Since the phases synthesized by IM are through a solid-solid transition, the structural compatibility between the newly formed phase and the matrix frequently plays an important role in determining whether the new phase can grow or not.[47] The Y-rich fcc-I phase, in the present case, was formed from an amorphous matrix, which was believed to have been formed through a traditional nucleation and growth mechanism. The fcc-I phase, however, was still closely related with the matrix metal, i.e., Y, in some structural characteristics. As the atomic arrangement of the hcp and fcc structures is quite similar on the closely packed planes, i.e., $\{111\}_{\rm fcc}$ and $\{0001\}_{\rm hcp}$ planes, the transition of hcp$\rightarrow$fcc can easily be realized by a sliding on the $\{0002\}_{\rm hcp}$ plane along the $\langle 1\bar{1}00\rangle_{\rm hcp}$ direction by a vector of $\frac{1}{3}\langle 1\bar{1}00\rangle_{\rm hcp}$. From this sliding mechanism, the relationship between the two lattices can be deduced as $a_{\rm fcc}=\sqrt{2}a_{\rm hcp}$. Using the lattice parameter of the pure yttrium of $a_{\rm hcp}=3.65$ Å, the lattice parameter of the fcc-I phase is calculated to be $a_{\rm fcc}=5.16$ Å. Compared with the experimental value of 5.10 Å, the error is less than 2%.

Generally, direct transformation from a bcc to a fcc structure is somewhat difficult. A two-step transition, i.e., bcc$\rightarrow$hcp$\rightarrow$fcc,[48,49] however, can easily proceed under IM and was indeed observed in the Mo-rich $Y_{15}Mo_{85}$ films. From a crystallographic point of view, the first step of bcc$\rightarrow$hcp can be fulfilled by a shearing which leads to a relationship of $a_{\rm hcp}=(\sqrt{3/2})a_{\rm bcc}$.[50] The second step of hcp$\rightarrow$fcc, following the above discussion, can be realized by a sliding and results in $a_{\rm fcc}=\sqrt{2}a_{\rm hcp}$. The lattice-parameter relationship between the fcc and the bcc lattices is therefore deduced as $a_{\rm fcc}=(\sqrt{6/2})a_{\rm bcc}$. Using Vegard's law, the lattice parameter of a $Y_{15}Mo_{85}$ supersaturated solid solution is about 3.35 Å; the lattice parameter of the fcc-II phase is thus calculated to be 4.10 Å. Compared with the experimental value of 4.04 Å, the difference between them is less than 2%. For the hcp-I and fcc-II phases in other samples which were from an amorphous matrix, the formation was through a traditional nucleation and growth mechanisms.

IV. CONCLUDING REMARKS

(1) Amorphization was achieved in the Y-Mo system by 200-keV xenon ion mixing at room temperature within two isolated composition ranges, i.e., Y_{22}–Y_{27} and Y_{72}–Y_{83}. In addition, three MX phases, i.e., Y-rich fcc-I and Mo-rich hcp-I and fcc-II, were formed.

(2) A Gibbs-free-energy diagram of the Y-Mo system was established by calculating the free-energy curves of the phases, especially including those of the three MX phases.

(3) Steady-state thermal annealing of the Y-Mo multilayered films with certain compositions was conducted. The annealing results revealed the relative energetic levels of the MX phases and in turn confirmed the relevance of the calculated free-energy diagram.

(4) The interfacial free energy of the as-deposited Y-Mo multilayers was calculated by using Gerkema and Miedema's model with varying number of interfaces. The calculated diagram together with the interface energies can give appropriate interpretation of the amorphization behavior and the GFA, and the formation of the three MX phases.

(5) The formation kinetics of the MX phases were considered to proceed via some solid-solid transition mechanisms and the lattice parameters so deduced agreed well with the experimental ones.

ACKNOWLEDGMENTS

The authors are grateful to the researchers in the TEM laboratory of the Peking University and the staff at the Analysis Center of Tsinghua University. Financial aid from the National Natural Science Foundation of China and from the Fundamental Research Foundation of Tsinghua University is acknowledged. The authors want to thank J. G. Sun and Z. Y. Zhao at the General Research Institute of Nonferrous Metals for their help in carrying out some experiments.

*Also at Center of Condensed Matter and Radiation Physics, CCAST (World Laboratory), Beijing 100080, China.

[1]G. Was, Prog. Surf. Sci. **32**, 211 (1989).
[2]L. S. Hung, M. Nastasi, J. Gyulai, and J. W. Mayer, Appl. Phys. Lett. **42**, 672 (1983).
[3]M. Nastasi, L. S. Hung, and J. W. Mayer, Appl. Phys. Lett. **43**, 831 (1983).
[4]J. L. Brimhall, H. E. Kissinger, and L. A. Charlot, in *Metastable Materials Formation by Ion Implantation,* edited by S. T. Picraux and W. J. Choyke, The MRS Symposia, Proceedings No. 7 (North-Holland, New York, 1982), p. 235.
[5]B. Y. Tsaur, S. S. Lau, and J. W. Mayer, Appl. Phys. Lett. **36**, 823 (1980).
[6]B. X. Liu, Vacuum **42**, 75 (1991).
[7]B. X. Liu, H. Y. Bai, Z. J. Zhang, and Q. L. Qiu, J. Alloys Compounds **196**, 37 (1993).
[8]H. U. Krebs, D. J. Webb, and A. F. Marshall, Phys. Rev. B **35**, 5393 (1987).
[9]D. G. Morris, Acta Metall. **31**, 1497 (1983).
[10]K. T.-Y. Kung, B. X. Liu, and M. A. Nicolet, Phys. Status Solidi A **77**, 355 (1983).
[11]B. X. Liu and M. A. Nicolet, Thin Solid Films **101**, 201 (1983).
[12]D. A. Lilienfeld, M. Nastasi, H. H. Johnson, D. G. Ast, and J. W. Mayer, Phys. Rev. Lett. **55**, 1587 (1985).
[13]D. A. Lilienfeld, M. Nastasi, H. H. Johnson, D. G. Ast, and J. W. Mayer, J. Mater. Res. **1**, 237 (1986).
[14]J. A. Knapp and D. M. Follstaedt, Phys. Rev. Lett. **55**, 1591 (1985).
[15]D. M. Follstaedt and J. A. Knapp, Phys. Rev. Lett. **56**, 1827 (1986).

[16]B. Y. Tsaur, S. S. Lau, L. S. Hung, and J. W. Mayer, Nucl. Instrum. Methods **182/183**, 67 (1981).
[17]Z. J. Zhang and B. X. Liu, J. Phys. Condens. Matter **6**, 9065 (1994).
[18]B. X. Liu, Phys. Status Solidi A **75**, K77 (1983).
[19]B. X. Liu, M. A. Nicolet, and S. S. Lau, Phys. Status Solidi A **73**, 183 (1983).
[20]J. A. Alonso, L. J. Gallego, and J. A. Somozar, Nuovo Cimento, **12**, 587 (1990).
[21]Z. J. Zhang and B. X. Liu, J. Appl. Phys. **76**, 3351 (1994).
[22]C. L. Chien, Phys. Rev. B **33**, 3243 (1986).
[23]K. Affolter, M. V. Allmen, H. P. Weber, and M. Witter, J. Non-Cryst. Solids **55**, 387 (1983).
[24]S. Simozar and J. A. Alonso, Phys. Status Solidi A **81**, 55 (1984).
[25]J. A. Alonso, L. J. Gallego, and J. M. Lopez, Philos. Mag. A **58**, 79 (1988).
[26]L. J. Gallego, J. A. Somozar, J. A. Alonso, and J. M. Lopez, Physica B **154**, 82 (1988).
[27]J. A. Alonso, L. J. Gallego, J. A. Somozar, and B. X. Liu, in *Thin films and Beam-Solid Interactions,* edited by L. Hung (Elsevier, Amsterdam, 1991), p. 197.
[28]L. J. Gallego, J. A. Somozar, H. M. Pernandez, and J. A. Alonso, in *Ordering and Disordering in Alloys,* edited by A. R. Yavari (Elsevier, London, 1992), p. 328.
[29]B. X. Liu and Z. J. Zhang, Phys Rev. B **49**, 12 519 (1994).
[30]R. B. Schwarz and J. B. Rubin, J. Alloys Compounds **194**, 189 (1993).
[31]A. R. Miedema, P. F. de Chatel, and F. R. De Boer, Physica B **100**, 1 (1980).
[32]A. K. Niessen and F. R. de Boer, J. Less-Common Met. **82**, 75 (1981).
[33]J. M. Lopez and J. A. Alonso, Z. Naturforsch. Teil A **40**, 1199 (1985).
[34]A. K. Niessen, F. R. de Boer, R. Boom, P. F. de Chatel, W. C. M. Matters, and A. R. Miedema (unpublished).
[35]R. Boom, F. R. de Boer, A. K. Niessen, and A. R. Miedema, Physica B **115**, 285 (1983).
[36]F. R. de Boer, A. R. Miedema, and R. Boom, Physica B **113**, 18 (1982).
[37]F. R. de Boer, R. Boom, W. C. M. Matters, A. R. Miedema, and A. K. Niessen, *Cohesion in Metals: Transition Metal Alloys* (North-Holland, Amsterdam, 1988), Chap. III.
[38]A. K. Niessen and A. R. Miedema, Ber. Bunsenges. Phys. Chem. **87**, 717 (1983).
[39]A. K. Niessen, A. R. Miedema, F. R. de Boer, and R. Boom, Physica B **151**, 401 (1988).
[40]B. X. Liu, Z. J. Zhang, and H. Y. Bai, J. Non-Cryst. Solids **156-158**, 603 (1993).
[41]Z. J. Zhang, H. Y. Bai, Q. L. Qiu, T. Yang, K. Tao, and B. X. Liu, J. Appl. Phys. **73**, 1702 (1993).
[42]C. Gente, M. Oehring, and R. Bormann, Phys. Rev. B **48**, 13 244 (1993).
[43]B. M. Clemens and T. C. Hufnagel, J. Alloys Compounds **194**, 221 (1993).
[44]J. Gerkema and A. R. Miedema, Surf. Sci. **124**, 351 (1981).
[45]F. Z. Cui, Y. D. Fan, Y. Wang, A. M. Vredenberg, H. J. G. Draaisma, and R. Xu, J. Appl. Phys. **68**, 701 (1990).
[46]M. W. Thompson, *Defects and Radiation Damage in Metals* (Cambridge University Press, Cambridge, England 1969), Chaps. 4 and 5.
[47]Z. J. Zhang and B. X. Liu, J. Phys. Condens. Matter **6**, 2647 (1994).
[48]Z. J. Zhang and B. X. Liu, J. Appl. Phys. **75**, 4948 (1994).
[49]B. X. Liu and Z. J. Zhang, J. Mater. Res. **9**, 3567 (1994).
[50]W. G. Burgers, Physica **1**, 561 (1934).

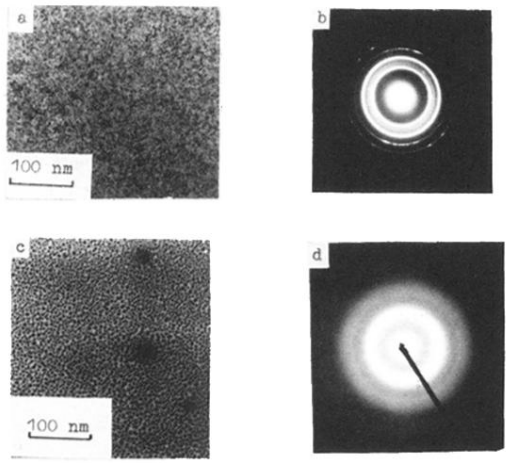

FIG. 1. (a) and (b) show a bright-field image and a corresponding SAD pattern of the as-deposited $Y_{72}Mo_{28}$ multilayers; (c) and (d) show a typical bright image and the corresponding SAD pattern of the amorphized multilayers at an irradiation dose of 3×10^{15} Xe^{+}/cm^{2} by room-temperature 200-keV xenon ion mixing.

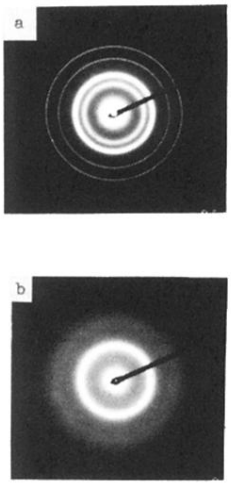

FIG. 2. (a) and (b) are the SAD patterns of the as-deposited $Y_{22}Mo_{78}$ multilayers and the corresponding amorphous phase formed by 200-keV room-temperature xenon ion mixing to a dose of 1×10^{15} Xe^{+}/cm^{2}.

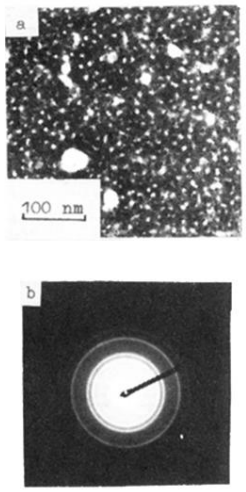

FIG. 3. (a) and (b) show a typical bright image and a corresponding SAD pattern of the Y-rich fcc-I MX phase formed in the $Y_{83}Mo_{17}$ multilayers by 200-keV xenon ion mixing to a dose of 7×10^{15} Xe^{+}/cm^{2} at room temperature.

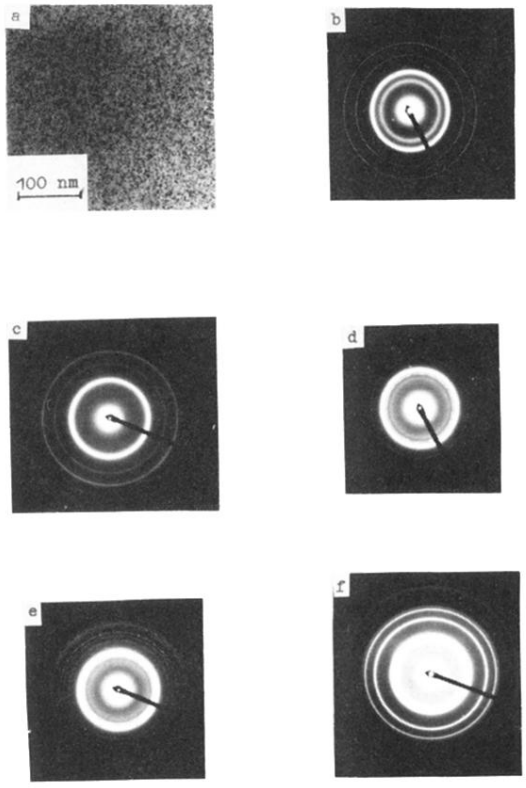

FIG. 4. (a),(b) Morphology and corresponding SAD pattern of the as-deposited $Y_{15}Mo_{85}$ multilayered films. (c)–(f) are the SAD patterns of the films at different irradiation stages upon 200-keV xenon ion mixing at room temperature: (c) a bcc solid solution formed at 1×10^{15} Xe^+/cm^2; (d) a hcp-I MX phase formed at 3×10^{15} Xe^+/cm^2; (e) a mixture of (hcp-I + fcc-II) formed at a dose of 5×10^{15} Xe^+/cm^2; and (f) a unique fcc-II MX phase formed at 7×10^{15} Xe^+/cm^2.

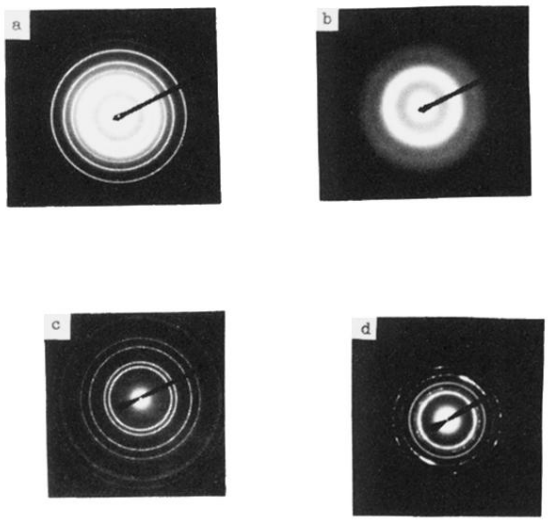

FIG. 6. SAD patterns of the $Y_{72}Mo_{28}$ multilayered films upon steady-state thermal annealing: (a) as deposited; (b) amorphized at 250 °C for 90 min; (c) the fcc-I MX phase formed after annealing at 350 °C for 30 min; and (d) the (Y + Mo) mixture reemerged when the temperature reached 600 °C and stayed for 60 min.

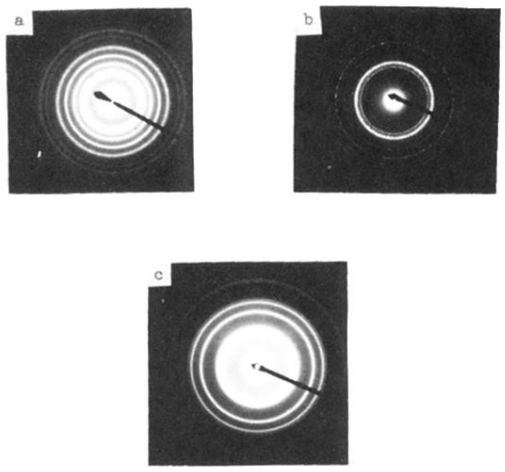

FIG. 7. SAD patterns of the $Y_{22}Mo_{78}$ multilayered films at different annealing stages: (a) as deposited; (b) the hcp-I MX phase formed after annealing at 500 °C for 60 min; and (c) the fcc-II MX phase formed after further annealing at 600 °C for 60 min.

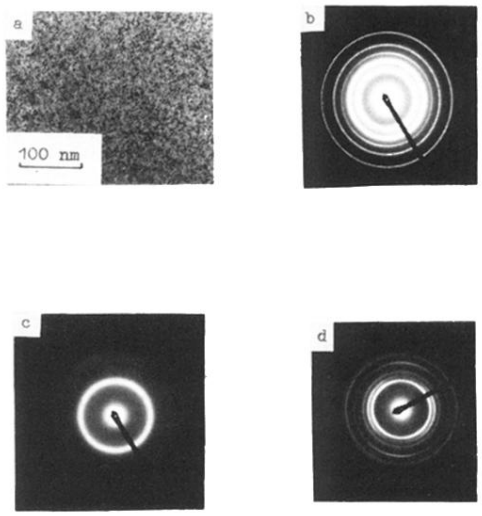

FIG. 9. (a) and (b) exhibit a typical morphology and a corresponding SAD pattern of the as-deposited N19 sample; (c) and (d) are the SAD patterns of the amorphized N19 sample at 350°C, and the reemerged (Y+Mo) mixture at 650°C, respectively.